Available online at www.eccomasproceedia.org
Eccomas Proceedia SMART (2023) 1635-1645

ECCOMAS
Proceedia

X ECCOMAS Thematic Conference on Smart Structures and Materials
SMART 2023
D.A. Saravanos, A. Benjeddou, N. Chrysochoidis and T. Theodosiou (Eds)

TOWARDS WHITE-BOX MODELING OF SENSORY-UTILIZED ROLLING BEARINGS

Steffen Puchtler*, Julius van der Kuip* and Eckhard Kirchner*

*Technical University of Darmstadt
Institute for Product Development and Machine Elements (pmd)
Otto-Berndt-Str. 2, 64287 Darmstadt, Germany
e-mail: office@pmd.tu-darmstadt.de, web page: https://www.pmd.tu-darmstadt.de/

Abstract. Most machines contain rolling element bearings. Thus, utilizing these machine elements as sensors is a huge opportunity for sensor integration without increasing design space or weakening the structure. The electrical impedance of a rolling bearing operated in hydrodynamic lubrication conditions mainly depends on the bearing's capacitance, as a usually non-conductive lubricant separates the surfaces of rolling elements and raceways. This capacitance depends on the Hertz'ian area and the lubrication film thickness, which are in turn functions of the bearing load. Thus, the bearing can be utilized as a load sensor. In this study, recent improvements to the capacitance model are discussed and compared with experimental results, marking considerable progress towards white-box models of rolling bearings utilized as load sensors and enabling simple sensor integration of load sensors in rotating machines close to the process and hence the zone of interest.

Key words: Rolling Bearing, Sensor Integration, White-Box Model

1 INTRODUCTION

The sensor-based use of the electrical properties of rolling bearings is becoming increasingly important as a potentially area-wide concept for accelerating digitization [1]. To this end, black box models, usually realized with machine learning algorithms, can reproduce the behavior of the data they were trained with. White box models that could be used for arbitrary lubricants, geometries, etc. are currently being improved [2, 3, 4]. Thus, influences on the capacitance, which were previously represented by rather inaccurate constant influence factors [5, 6], could be replaced for the point contact by phenomenological equations for the respective operating state, [3, 4, 7]. The electrical impedance of rolling bearings in fluid film lubrication depends on the capacitance of the rolling contacts. Figure 1.a shows an example of a capacitance network of a deep groove ball bearing with a conductive cage, according to [8].

Under radial load, the various rolling elements experience different forces, and a load zone is formed. Opposite the load zone, there are unloaded rolling elements in the rolling bearing with clearance at low axial loads. In the loaded rolling elements, Figure 1.b, a Hertz'ian contact

Peer-review under responsibility of the organizing committee of SMART 2023.
doi: 10.7712/150123.9935.444456

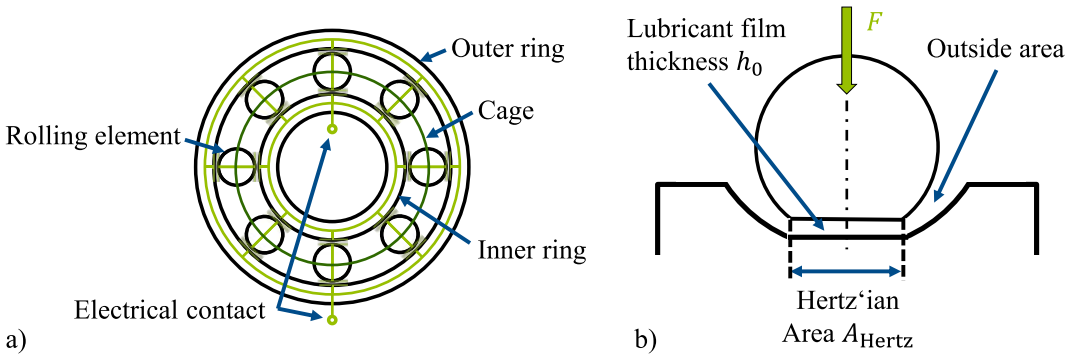

Figure 1: Representation of the deep groove ball bearing as a capacitance network: a) individual capacitances of the rolling contacts with conductive cage, b) Hertz'ian area of the loaded single contact [9].

area A_{Hertz} with the central lubricant film thickness h_0 is formed, while the unloaded rolling elements remain undeformed between the inner and outer ring. In rolling bearing applications with a fully formed lubricant film in the load zone, the relevant electrical quantity for describing the electrical behavior is the capacitance, since the metallic bodies are separated from each other and common lubricants exhibit a very high resistivity [10]. Thus, the lubricant acts as a dielectric, and the rolling elements and raceway form electrodes. In this work, the full procedure for calculating the mentioned capacitance is displayed, and results are discussed and compared with measurement results.

2 MATERIALS AND METHODS

In this section, the proposed bearing capacitance model is explained in detail. Inverting this model delivers a white box model using relevant input parameters like the measured impedance, the rotational speed, and oil temperature to calculate lubrication film thickness or bearing load. Basic input parameters to the forward model, besides the bearing geometry and materials, Table 1 and lubricant parameters, Table 2, are:

- the radial load F_{r} and
- the axial load F_{a} acting on the bearing,
- the rotational speed n of the inner ring assuming the outer ring is at standstill,
- the temperature T_{Oil} of the oil when entering the bearing and
- the diametral clearance P_{d} under operation conditions.

2.1 Bearing Geometry

All required input parameters for the bearing geometry and material are listed in Table 1.

Table 1: Bearing geometry and material parameters of a 6205 deep groove ball bearing.

Symbol	Parameter	Value
d	Basic bore diameter	$25\,\mathrm{mm}$
D	Basic outside diameter	$52\,\mathrm{mm}$
D_{RE}	Rolling element diameter	$7.938\,\mathrm{mm}$
B	Basic width	$15\,\mathrm{mm}$
Z	Number of rolling elements	9
f_i	Inner race conformity ratio	0.52
f_o	Outer race conformity ratio	0.53
B_i	Width of inner race	$5.03\,\mathrm{mm}$
B_o	Width of outer race	$4.82\,\mathrm{mm}$
E_{St}	Young's modulus	$207\,\mathrm{GPa}$
ν_{St}	Poisson's ratio	0.3
$\alpha_{\mathrm{t,St}}$	Thermal heat expansion coefficient	$1.15 \times 10^{-5}\,\mathrm{K}^{-1}$
ϱ_{St}	Density	$7810\,\mathrm{kg\,m}^{-3}$

First, in order to calculate basic geometry parameters, the free contact angle α needs to be calculated. It describes the angle between the ball-to-raceway contact point and the radial axis at a minimal axial and no radial load. It depends on the bearing's clearance P_{d}, the rolling element diameter D_{RE} and the race conformity ratios f_{i} and f_{o} via the dimensionless distance between the race radii center points, $B_{\mathrm{m}} = f_{\mathrm{i}} + f_{\mathrm{o}} - 1$, [11],

$$\alpha = \arccos\left(1 - \frac{P_{\mathrm{d}}}{2B_{\mathrm{m}}D_{\mathrm{RE}}}\right). \tag{1}$$

For each ball-on-race contact, the effective radii resulting from the Hertz'ian theory [12] are calculated according to [13],

$$R_{\mathrm{x,i}} = \frac{D_{\mathrm{RE}}(d_{\mathrm{m}} - D_{\mathrm{RE}}\cos\alpha)}{2d_{\mathrm{m}}}\,,\; R_{\mathrm{x,o}} = \frac{D_{\mathrm{RE}}(d_{\mathrm{m}} + D_{\mathrm{RE}}\cos\alpha)}{2d_{\mathrm{m}}}\,, \tag{2}$$

$$R_{\mathrm{y,i}} = \frac{f_{\mathrm{i}}D_{\mathrm{RE}}}{2f_{\mathrm{i}} - 1}\,,\; R_{\mathrm{y,o}} = \frac{f_{\mathrm{o}}D_{\mathrm{RE}}}{2f_{\mathrm{o}} - 1}\,. \tag{3}$$

Thereby, R_x defines the effective radius in the rolling direction, and R_y the effective radius perpendicular to the rolling direction. The index i describes the contact on the inner ring, and o describes the contact on the outer ring. The bearing pitch diameter can be estimated as $d_{\mathrm{m}} = (d + D)/2$. Subsequently, the curvature sum R_{s} and curvature difference Γ can be calculated [13],

$$R_{\mathrm{s,i}} = \frac{R_{\mathrm{x,i}}R_{\mathrm{x,i}}}{R_{\mathrm{x,i}} + R_{\mathrm{x,i}}}\,,\; R_{\mathrm{s,o}} = \frac{R_{\mathrm{x,o}}R_{\mathrm{x,o}}}{R_{\mathrm{x,o}} + R_{\mathrm{x,o}}}\,, \tag{4}$$

$$\Gamma_\mathrm{i} = R_\mathrm{s,i}\left(\frac{1}{R_\mathrm{x,i}} - \frac{1}{R_\mathrm{y,i}}\right)\,,\ \Gamma_\mathrm{o} = R_\mathrm{s,o}\left(\frac{1}{R_\mathrm{x,o}} - \frac{1}{R_\mathrm{y,o}}\right)\,. \tag{5}$$

Then, for both, Hertz'ian contact deformation and lubrication film thickness calculations, the reduced Young's modulus of contact partners can be calculated from the Young's moduli E_RE and E_ring and the Poisson's ratios ν_RE and ν_ring [13],

$$E' = \frac{2}{\frac{1-\nu_\mathrm{RE}^2}{E_\mathrm{RE}} + \frac{1-\nu_\mathrm{ring}^2}{E_\mathrm{ring}}}\,. \tag{6}$$

2.2 Lubricant parameters

All required lubricant parameters are listed in Table 2.

Table 2: Lubricant parameters of reference oil FVA IIIa by *Forschungsvereinigung Antriebstechnik* (FVA, Research Association for Drive Technology).

Symbol	Parameter	Value
K	Vogel parameters	$7.084 \times 10^{-5}\,\mathrm{Pa\,s}$
B		$800.3\,^\circ\mathrm{C}$
C		$95\,^\circ\mathrm{C}$
ν_{38}	Kinematic viscosity at $38\,^\circ\mathrm{C}$ and ambient pressure	$34\,\mathrm{mm^2\,s^{-1}}$
α_p	Pressure viscosity coefficient	$23\,\mathrm{GPa^{-1}}$
λ	Heat conductivity	$0.133\,\mathrm{W\,m^{-1}\,K^{-1}}$
ϱ_el	Specific resistance	$1 \times 10^9\,\Omega\,\mathrm{m}$
ε_Oil	Relative permittivity	2.2

The temperature-dependent dynamic viscosity of the oil at ambient pressure can be calculated according to the Vogel–Fulcher–Tammann equation [14],

$$\eta_0 = K e^{\frac{B}{T_\mathrm{Oil}+C}}\,. \tag{7}$$

Measurements for the Vogel parameters K, B and C, cf. Table 2, can be retrieved from [15]. The remaining parameters in Table 2 will become relevant in the following calculations.

2.3 Load distribution

The load distribution is calculated using the temperature-dependent bearing geometry as well as the geometric intersection of undeformed contact partners, which results in contact forces. In addition to the deflection forces, hydrodynamic forces are calculated using the approach in Section 2.4, allowing to estimate the position of unloaded rolling elements. Then, the three-dimensional position of the inner ring in relation to the outer ring is varied till the equilibrium of forces is found. More details on the derivation of the load distribution model can be found in [7].

2.4 Lubricant film thickness

Next, for each of the $2Z = 18$ rolling contacts, i.e. Z inner and Z outer contacts, cf. Figure 1.a, the lubrication film thickness is calculated. The film thickness equation of Hamrock and Dowson [13] consists of four dimensionless parameters, which are described in the following. For the dimensionless speed parameter, the surface velocity u is required [13],

$$u = \frac{d_{\mathrm{m}}^2 - D_{\mathrm{RE}}^2 \cos^2 \alpha}{4 d_{\mathrm{m}}} 2\pi n \,. \tag{8}$$

With the dynamic viscosity η_0 (7), the reduced Young's modulus E' (6) and the reduced contact radius in rolling direction R_x (2), the dimensionless speed parameter U can be calculated [13],

$$U = \frac{\eta_0 u}{E' R_x} \,. \tag{9}$$

The dimensionless load parameter is calculated by dividing the rolling element load Q by the reduced Young's modulus E' and the reduced radius R_x squared [13],

$$W = \frac{Q}{E' R_x^2} \,. \tag{10}$$

With the pressure viscosity coefficient α_p and, again, the reduced Young's modulus E', the dimensionless material parameter G can be calculated [13],

$$G = \alpha_p E' \,. \tag{11}$$

With the ellipticity parameter $k = a/b$, which is the ratio of the semi axes of the Hertz'ian contact ellipse [12], finally the dimensionless central lubrication film thickness H_0 can be calculated [13],

$$H_0 = h_0 / R_x = 2.69\, U^{0.67}\, G^{0.53}\, W^{-0.067}\, (1 - 0.61 e^{-0.73k}) \,. \tag{12}$$

Then, a thermal correction of the calculated lubrication film thickness following Kreil is applied [16],

$$h_{0,\mathrm{th}} = h_0 \frac{3.94}{3.94 + L^{0.62}} \,, \tag{13}$$

using the thermal load factor L, which is calculated with the material parameter G (11) and the speed parameter U (9) [17],

$$L = G(2U)^{1/4} \,. \tag{14}$$

2.5 Capacitance calculation

Lastly, the capacitance of each of the 18 contacts is calculated, cf. Figure 1.a. The relatively high pressure in rolling contacts requires a pressure-dependent formulation of the lubricant permittivity provided by Schmidt [18],

$$\varepsilon'_{\mathrm{Oil}} = \frac{\varepsilon_{\mathrm{Oil}} + 2 + 2(\varepsilon_{\mathrm{Oil}} - 1)\frac{\varrho'}{\varrho_0}}{\varepsilon_{\mathrm{Oil}} + 2 - (\varepsilon_{\mathrm{Oil}} - 1)\frac{\varrho'}{\varrho_0}}\,, \tag{15}$$

with the density ratio ϱ'/ϱ_0 [18],

$$\frac{\varrho'}{\varrho_0} = 1 + \frac{9.73 \times 10^{-3}(0.101\,972 \times 10^{-6}\,p)^{0.75}}{(10^6\,\nu_{38})^{0.0385}}\,, \tag{16}$$

where ν_{38} is the kinematic viscosity at $38\,^{\circ}\mathrm{C}$, cf. Table 2, p the mean contact pressure retrieved by the Hertz'ian theory [12] and $\varepsilon_{\mathrm{Oil}}$ the lubricant's permittivity at ambient pressure, cf. Table 2. Then, the capacitance of each Hertz'ian contact ellipse is calculated,

$$C_{\mathrm{Hertz}} = \varepsilon_0 \varepsilon'_{\mathrm{Oil}} \frac{A_{\mathrm{Hertz}}}{h_{0,\mathrm{th}}}\,, \tag{17}$$

where $\varepsilon_0 = 8.8542 \times 10^{-12}\,\mathrm{F\,m^{-1}}$ is the vacuum permittivity, $A_{\mathrm{Hertz}} = \pi ab$ the area of the Hertz'ian contact ellipse, and $h_{0,\mathrm{th}}$ the thermally corrected lubrication film thickness (13).

The contribution of the area outside the Hertz'ian contact as well as the unloaded rolling elements C_{out} is calculated using a semi-analytic approximation derived in [19] and applied in [7]. Then, the total capacitance is calculated from all contact capacitances $C_{\mathrm{contact},j} = C_{\mathrm{Hertz},j} + C_{\mathrm{out},j}$ for loaded and $C_{\mathrm{el},j} = C_{\mathrm{out},j}$ for unloaded rolling elements and rolling element j with a conductive cage, cf. Figure 1,

$$C = \frac{1}{\frac{1}{\sum_{j=1}^{Z} C_{\mathrm{contact,i},j}} + \frac{1}{\sum_{j=1}^{Z} C_{\mathrm{contact,o},j}}}\,. \tag{18}$$

3 RESULTS AND DISCUSSION

In this section, the calculation results of the above-described capacitance model are shown, discussed, and later compared with measurement results.

3.1 Theoretical results

Figure 2 shows the calculated total capacitance as a contour plot with the radial load F_{r} on the horizontal axis and the axial load F_{a} on the vertical axis. The capacitance increases monotonically with both, radial and axial load. Three factors contribute to this behavior. Firstly, the lubrication film thickness h_0 (12) decreases with load $W \propto Q$ (10) even with a small exponent $h_0 \propto W^{-0.067}$ (12). Secondly, a higher impact results from the Hertz'ian area A_{Hertz} (17), which is increasing with the load as well. Thirdly, the permittivity of the oil $\varepsilon'_{\mathrm{Oil}}$ increases with pressure (15). Furthermore, an asymmetric influence of radial and axial loads can be

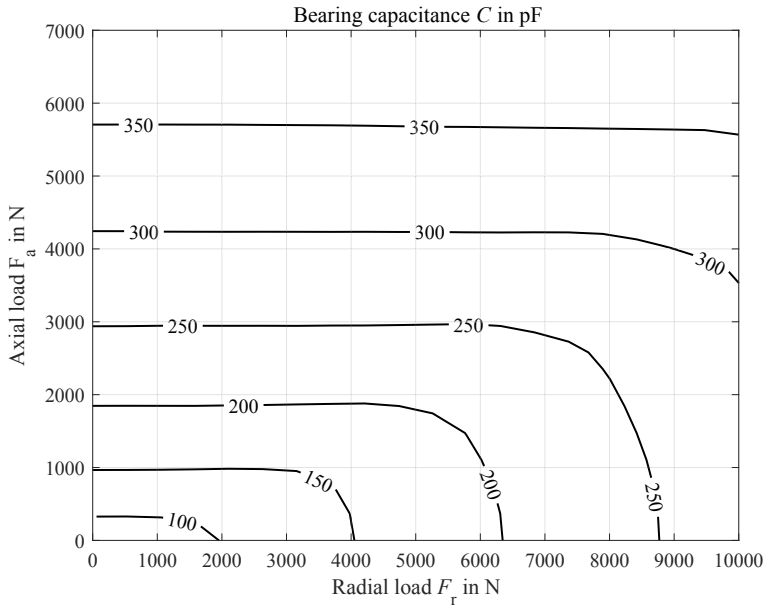

Figure 2: Total capacitance C of a 6205-C3 deep groove roller bearing under combined load in dependency of axial load F_a and radial load F_r at an oil temperature of $T_\mathrm{Oil} = 60\,^\circ\mathrm{C}$ and a rotational speed of $n = 3000\,\mathrm{rpm}$.

observed. For load angles $\beta = \arctan\left(F_\mathrm{r}/F_\mathrm{a}\right) \gtrapprox 70^\circ$ the influence of the radial load seems negligible. On the other hand, small axial loads have a higher influence on the total capacitance as more rolling elements bear load and thus contribute to the total capacitance.

Figure 3 shows the calculated bearing capacitance as a contour plot, with the oil temperature T_Oil on the vertical axis at pure radial load, $F_\mathrm{a} = 0$. The capacitance monotonically increases with the temperature. The temperature's influence on the lubricant film thickness is indirect, as the viscosity is highly dependent on the temperature. Thus, in the range of $T_\mathrm{Oil} = 20\,^\circ\mathrm{C}$ to $120\,^\circ\mathrm{C}$ the viscosity ranges from $\eta_0 = 0.005\,\mathrm{Pa\,s}$ to $0.283\,\mathrm{Pa\,s}$. Via the speed parameter U (9), the film thickness has a significant dependency on the dynamic viscosity $h_0 \propto U^{0.67} \propto \eta_0^{0.67}$. This influence is slightly limited by the thermal correction, (13). The temperature influence at higher loads doesn't affect the unloaded regions, which have a higher impact at low loads.

Figure 4 shows the calculated total capacitance with the rotational speed n on the vertical axis for pure radial load. An increasing rotational speed causes a decrease in capacitance, which is due to the higher lubricant film thickness at higher speeds, $h_0 \propto U^{0.67} \propto n^{0.67}$ (8),(9),(12).

3.2 Experimental results

Experiments were carried out at a bearing test rig at the authors' institute, which is described in detail in [7]. An electric motor drives a shaft with four deep groove roller bearings. Hydraulic cylinders apply a radial and an axial load on the shaft. The test bearing is a 6205-C3 bearing with a glass-fiber-reinforced polyamid PA66 cage, and the support bearings are hybrid bearings to reduce stay capacitances. FVA reference oil IIIa was used for lubrication at a volume flow

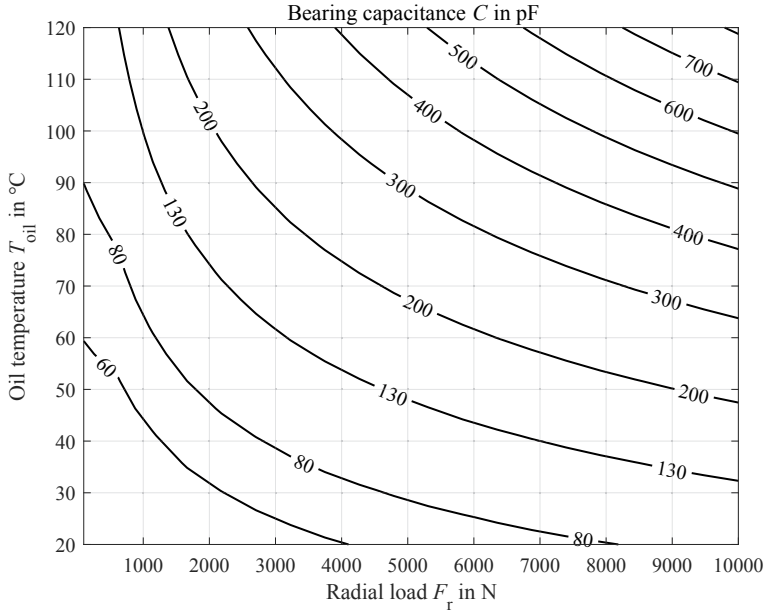

Figure 3: Total capacitance C of a 6205-C3 deep groove roller bearing under pure radial load F_r in dependency of the oil temperature T_Oil at a rotational speed of $n = 3000\,\mathrm{rpm}$.

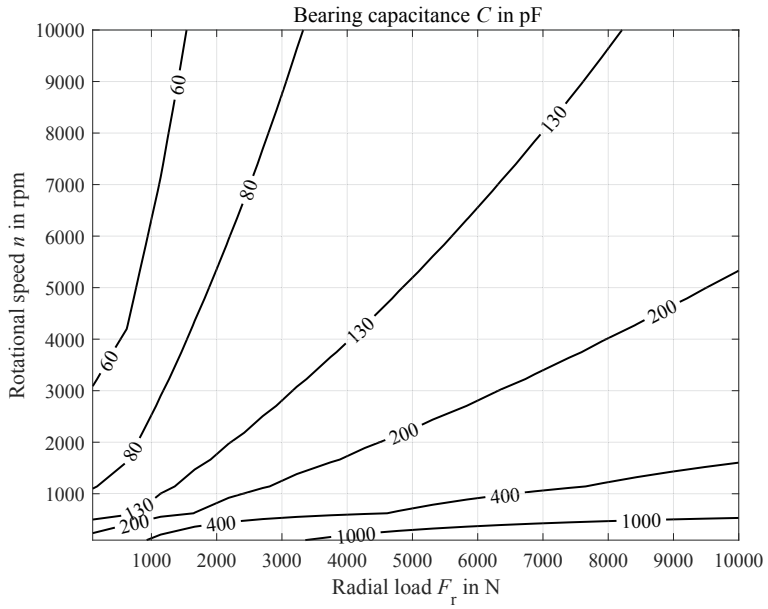

Figure 4: Total capacitance C of a 6205-C3 deep groove roller bearing under pure radial load F_r in dependency of the rotational speed n at an oil temperature of $T_\mathrm{Oil} = 60\,^\circ\mathrm{C}$.

rate of $10\,\mathrm{L/min}$ and preheated to the designated temperature T_Oil before being led into the test chamber. The loads were tested in a randomized order, but the oil temperature was not included in the randomization because of the long heating time and energy consumption. The

capacitance was measured at a carrier frequency of $f = 8\,\mathrm{kHz},\ 20\,\mathrm{kHz}$ and $100\,\mathrm{kHz}$ for $15\,\mathrm{s}$ each. Then, results were averaged, the standard deviation was calculated and displayed as error bars in Figure 5. The calculations are based on the actual sensor values of the test rig.

In Figure 5 a generally good agreement between the white box model and measurements, as compared to e.g. [4], can be observed. Measurements at $T_{\mathrm{Oil}} = 90\,^{\circ}\mathrm{C}$ show a higher deviation for higher loads. This might be due to partial mixed lubrication, where the surface roughness of the contact partners becomes relevant, which is not accounted for in the current model. On the other hand, deviations at very low loads at the load angle $\beta = 15^{\circ}$ can be observed. This is due to the hydraulic system applying the axial load, which is not capable of setting an axial load as low as required. Subsequently, the actual load angle at low loads is greater than 15°. For a statistically meaningful result, more bearings of the same kind should be tested. This would also help to decrease the standard deviation of some test points.

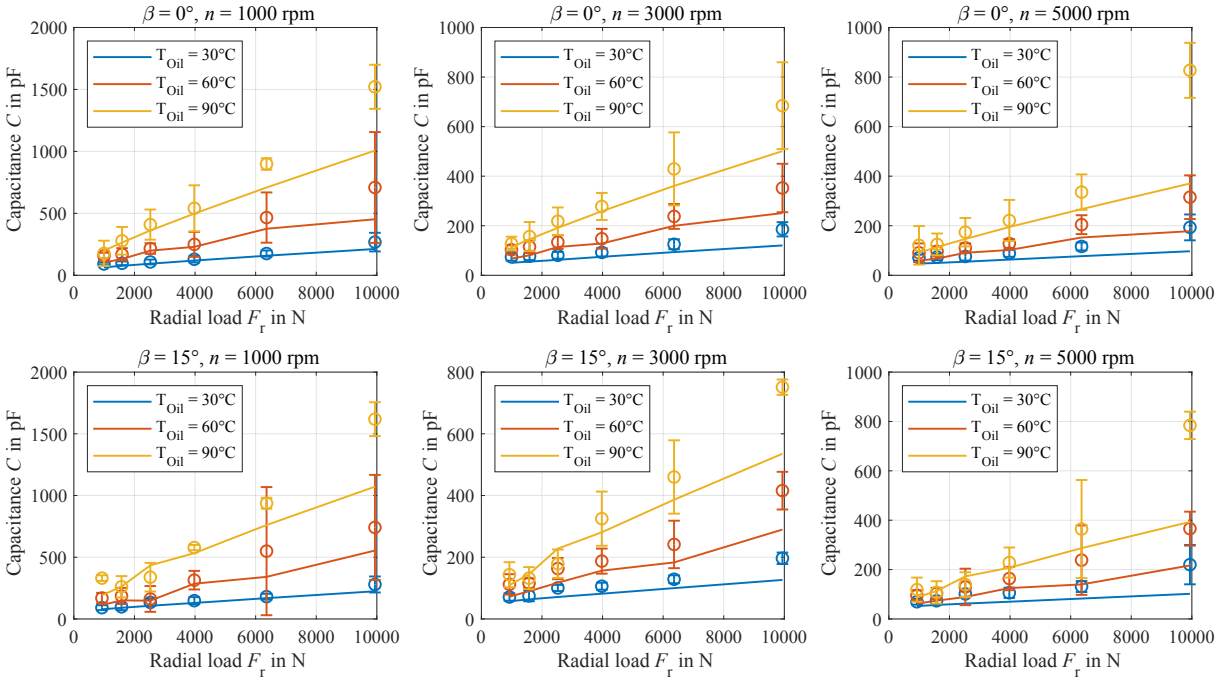

Figure 5: Measured (circles with error bars) and calculated (line) capacitance C of a 6205-C3 deep groove roller bearing for different oil temperatures T_{Oil}, load angles $\beta = \arctan\left(F_{\mathrm{r}}/F_{\mathrm{a}}\right)$ and rotational speeds n in dependency of the radial load F_{r}.

4 CONCLUSION

In this work, the current state of a continuously improved white box model of a sensory-utilizable deep groove ball bearing has been presented. The proposed model does not rely on black box approaches, which either work for a limited number of bearing geometries and lubricants or require an excessive amount of data for training all relevant parameters. Unlike

previous work, it also omits any correction factors for capacitance calculation and describes the physical behavior well, as seen in a comparison of calculation results with corresponding measurements. Thus, this work marks a further step towards a full understanding of the electrical behavior of ball bearings and, therefore, towards the white box modeling of sensory-utilized rolling bearings.

ACKNOWLEDGEMENTS This work was funded by the Deutsche Forschungsgemeinschaft (DFG, German Research Foundation) – 467849890

REFERENCES

[1] T. Schirra, G. Martin, M. Neu, and E. Kirchner, "Feasibility study of impedance analysis for measuring rolling bearing loads," Nashville, 2019. [Online]. Available: https://www.stle.org/images/pdf/STLE_ORG/AM2019%20Presentations/Contact%20Mechanics/STLE2019_Contact%20Mechanics%20II_Session%208I_T.%20Schirra_Feasibility%20Study%20of%20Impediance%20Analysis.pdf

[2] K. Jabłonka, R. Glovnea, J. Bongaerts, and G. Morales-Espejel, "The effect of the polarity of the lubricant upon capacitance measurements of EHD contacts," *Tribology International*, vol. 61, pp. 95–101, 2013.

[3] V. Schneider, H.-C. Liu, N. Bader, A. Furtmann, and G. Poll, "Empirical formulae for the influence of real film thickness distribution on the capacitance of an EHL point contact and application to rolling bearings," *Tribology International*, vol. 154, p. 106714, 2021.

[4] T. Schirra, G. Martin, S. Puchtler, and E. Kirchner, "Electric impedance of rolling bearings - Consideration of unloaded rolling elements," *Tribology International*, vol. 158, p. 106927, 2021.

[5] Y. Gemeinder, M. Schuster, B. Radnai, B. Sauer, and A. Binder, "Calculation and validation of a bearing impedance model for ball bearings and the influence on EDM-currents," in *2014 International Conference on Electrical Machines (ICEM 2014)*. Piscataway, NJ: IEEE, 2014, pp. 1804–1810.

[6] A. Mütze, "Bearing Currents in Inverter-Fed AC-Motors," Dissertation, TU Darmstadt, Darmstadt, 2003.

[7] S. Puchtler, J. van der Kuip, and E. Kirchner, "Analyzing Ball Bearing Capacitance Using Single Steel Ball Bearings," *Tribology Letters*, vol. 71, no. 2, 2023.

[8] H. Prashad, "Theoretical evaluation of Impedance, Capacitance and Charge Accumulation on Roller Bearings Operated under Electrical Fields," *Wear*, vol. 125, no. 3, pp. 223–239, 1988.

[9] S. Puchtler, T. Schirra, E. Kirchner, Y. Späck-Leigsnering, and H. de Gersem, "Effiziente Berechnung des elektrischen Feldes im Wälzkontakt: Beitrag zur Ermittlung der elektrischen Impedanz," in *Gleit- und Wälzlagerungen 2021*, ser. VDI-Berichte. Düsseldorf: VDI Verlag GmbH, 2021, pp. 75–86.

[10] D. Bechev, "Prüfmethodik zur Charakterisierung der elektrischen Eigenschaften von Wälzlagerschmierstoffen," Dissertation, TU Kaiserslautern, Kaiserslautern, 2020.

[11] T. A. Harris and M. N. Kotzalas, *Essential concepts of bearing technology*, 5th ed., ser. Rolling bearing analysis / Tedric A. Harris Michael N. Kotzalas. Boca Raton, London, New York: CRC Press, 2007, vol. 1.

[12] H. Hertz, "Über die Berührung fester elastischer Körper," *Journal für die reine und angewandte Mathematik*, no. 92, pp. 156–171, 1881.

[13] B. J. Hamrock and D. Dowson, *Ball bearing lubrication: The elastohydrodynamics of elliptical contacts*. New York: Wiley, 1981.

[14] G. S. Fulcher, "Analysis of recent Measurements of the Viscosity of Glasses," *American Ceramic Society (Journal of the American Ceramic Society)*, vol. 8, no. 6, pp. 339–355, 1925.

[15] Forschungsvereinigung Antriebstechnik e.V., "Schmierfilmdicke: Einfluss von Grundölart, Additivierung und Gebrauchszustand auf Viskositätsverhalten und Schmierfilmbildung: Forschungsvorhaben Nr. 400," no. 743, 2004.

[16] O. Kreil, "Einfluss der Oberflächenstruktur auf Druckverteilung und Schmierfilmdicke im EHD-Kontakt," Dissertation, TU München, München, 2009.

[17] M. Marian, M. Bartz, S. Wartzack, and A. Rosenkranz, "Non-Dimensional Groups, Film Thickness Equations and Correction Factors for Elastohydrodynamic Lubrication: A Review," *Lubricants*, vol. 8, no. 10, p. 95, 2020.

[18] U. Schmidt, "Die Schmierfilmbildung in elastohydrodynamisch Beanspruchten Wälzkontakten unter Berücksichtigung der Oberflächenrauheit," Dissertation, Universität Hannover, Hannover, 1985.

[19] S. Puchtler, T. Schirra, E. Kirchner, Y. Späck-Leigsnering, and H. de Gersem, "Capacitance calculation of unloaded rolling elements – Comparison of analytical and numerical methods," *Tribology International*, vol. 176, p. 107882, 2022.